



# Combining resistivity and frequency domain electromagnetic methods to investigate submarine groundwater discharge (SGD) in the littoral zone

Marieke Paepen<sup>1</sup>, Daan Hanssens<sup>2</sup>, Philippe De Smedt<sup>2</sup>, Kristine Walraevens<sup>1</sup>, and Thomas Hermans<sup>1</sup>

5 <sup>1</sup>Laboratory of Applied Geology and Hydrogeology, Department of Geology, Ghent University, Krijgslaan 281-S8, Ghent, 9000, Belgium

<sup>2</sup>Research Group Soil Spatial Inventory Techniques, Department of Soil Management, Ghent University, Coupure links 653, Ghent, 9000, Belgium

*Correspondence to:* M. Paepen (Marieke.Paepen@UGent.be)

10 **Abstract.** Submarine groundwater discharge (SGD) is an important gateway for nutrients and pollutants from land to sea. The study of SGD is thus important for nearshore ecosystems and the management of coastal freshwater reserves. The discharge occurs at the limit between land and sea, a dynamic environment, making the assessment difficult. And more important, SGD is characterized by a significant spatial and temporal variability. Therefore, a variety of techniques and measurements in multiple periods is needed to capture the magnitude of SGD in one particular site. To detect zones of discharge, we combine  
15 several geophysical methods in the intertidal zone, as well as on the upper beach, in the dunes, and shallow coastal area. Electrical resistivity tomography (ERT) – on land, roll-along ERT and on sea, marine continuous resistivity profiling (CRP) – is used from the shallow continental shelf up to the dunes, combined to frequency domain electromagnetics (FDEM) mapping in the intertidal zone. The highly saline environment we work in causes FDEM instruments operated under low induction  
20 number (LIN) to underestimate the apparent electrical conductivity (ECa). Here, we apply a quadrature-phase algorithm to obtain a robust ECa (rECa), valid at low and high induction numbers. ‘De Westhoek’ (Belgium) was chosen as a test site, which is bordered by the North Sea. It is a strong dynamic environment, with semi-diurnal tides between 3 and 5 m. Providing approximately 6 hours between low and high tide, this leaves little time to work close to the low water line. CRP is usually applied in calmer conditions, but we prove that a survey is possible on the North Sea, providing additional information to the  
25 ERT survey which is mainly restricted to the land. The 2D inversion models created from ERT and CRP data clearly indicate the presence of SGD on the lower beach (in the East) or below the low water line (in the West of the study area). The discharge originates from a potable freshwater lens underneath the dunes, which delimit the sandy beach. The fresh groundwater flows underneath a thick saltwater lens, present from the dunes to the lower beach, which is fully observed with ERT. FDEM mapping reveals discharge at the same locations and clearly displays the lateral variation of the zone of discharge. ERT, CRP, and FDEM are complementary tools in the investigation of SGD. They provide a high-resolution 3D image of the salt and  
30 freshwater distribution in phreatic coastal aquifer over a relatively large area, both off- and onshore.



## 1 Introduction

The interface between land and sea is a complex environment, with groundwater discharging from the land and salt water intruding into coastal aquifers. Submarine groundwater discharge (SGD) and seawater intrusion (SI) are complementary processes, both subjected to the balance between hydraulic and density gradients in ground- and seawater (Taniguchi et al., 2002). SGD is a combination of fresh SGD and recirculated saline groundwater discharge (RSGD) (Taniguchi et al., 2002). It is driven by the terrestrial hydraulic gradient, water level differences at permeable barriers, wave set-up, tides, storm or current-induced pressure gradients, convection, seasonal fresh-seawater interface movement, and geothermal heating (Taniguchi et al., 2002 ; Michael et al., 2005 ; Burnett et al., 2006). Its total flux is significant, since it occurs over large areas (Burnett et al., 2003), probably being more important to the oceanic budgets of nutrients, carbon, and metals than rivers (Moore, 2010).

SGD can lead to eutrophication (e.g. Colman et al., 2004 ; Hwang et al., 2005), blooms of harmful algae (e.g. Lapointe et al., 2005), and it can result in a significant loss of **freshwater**. On the other hand, SI threatens potable water in coastal zones. Therefore, understanding the dynamics of salt and freshwater is essential for management of coastal freshwater reserves. However, assessment of SGD is difficult, because of spatial and temporal variability in flux (e.g. **Burnett & Dulaiova, 2003 ; Michael et al.; 2005**). Geophysical techniques can be used to delineate salt and freshwater in coastal environments, facilitating the detection of SGD and SI. Electrical and electromagnetic methods are particularly suited for spatial and temporal salinity delineation in coastal environments given their sensitivity to (water) electrical conductivity.

Time domain electromagnetic (TDEM) measurements have been used to measure salinity onshore (e.g. Goldman et al., 1991 ; Kontar & Ozorovich, 2006) or offshore, using a floating system (e.g. Goldman et al., 2004). Also FDEM can be used offshore, by towing transmitter and receiver with a boat on the seafloor (Evans et al., 1999 ; Hoefel and Evans, 2001). Ground conductivity instruments designed to operate under low induction number conditions (LIN) (e.g. CMD-MiniExplorer, DUALEM-421S, Geonics EM34, and EM31) provide apparent electrical conductivities (ECa) which are not valid in highly conductive environments (McNeill, 1980 ; Hanssens et al., 2019), which is probably why the technique has rarely been applied in the intertidal zone. Only the ECa values were used in the interpretation of all following cited FDEM studies. Greenwood et al. (2006) acquired pore water salinity in a coastal wetland on Tampa Bay, Florida, with the EM31 and EM34. Pauw (2009) used the EM34 in combination with (continuous) vertical electrical and TDEM soundings, to investigate the distribution of salt and freshwater between Egmond aan Zee and Castricum aan Zee (the Netherlands). Obikoya & Bennell (2012) combined EM31 with 2D resistivity imaging to detect plumes of freshwater on the beach (North Wales). The DUALEM-421 was used by Davies et al. (2015) to map saltwater intrusion on Long Reef beach. Francés et al. (2015) combined the EM34 with TDEM and onshore electrical resistivity tomography (ERT), to discriminate between fresh and salt water in order to update the hydrogeological conceptual model of the Albufeira-Ribeira de Quarteira coastal aquifer system (Portugal). Additionally, FDEM has been used for archaeological prospection (Delefortrie et al., 2014a ; Bonsall & Dowd, 2015), to facilitate palaeoenvironmental reconstruction (Bates & Bates, 2016), and to characterize the beach thickness in combination with ERT, ground penetrating radar, continuous surface waves, etc. (Gunn et al., 2006). Both FDEM and TDEM methods are also



available for airborne surveys, allowing to expand the coverage in coastal and tidal environments, see Siemon et al. (2009) and Viezzoli et al. (2012) for some examples. These surveys can be combined with for instance EM (e.g. Paine, 2003) or ERT studies on land (e.g. Viezzoli et al., 2010 ; Goebel et al., 2019).

Next to EM, ERT is a useful method in mapping coastal salinity. For example, Dimova et al. (2012) used a shoreline parallel ERT profile to identify at which moment in the tidal cycle the groundwater exchange is largest from a volcanic coastal aquifer to Kiholo Bay (Hawaii). Goebel et al. (2017) gathered extremely long ERT lines above the high tide line, imaging saltwater intrusion along Monterey Bay. Also, time lapse ERT is popular for monitoring saltwater intrusion (e.g. de Franco et al., 2009 ; Ogilvy et al., 2009). Coastal long-term time lapse cross-hole ERT was used to improve knowledge of **SI** at the Argenton site (Palacios et al., 2018).

Also, resistivity surveying in water is possible: by towing a streamer behind a boat (continuous resistivity profiling – CRP) or the cable is rested on/buried in the sediments (marine electrical resistivity – MER) (e.g. Swarzenski et al., 2006 ; Taniguchi et al., 2007 ; Swarzenski & Izbicki, 2009 ; Henderson et al., 2010). The latter provides a better resolution, since the water layer on top has less effect on the signal compared to CRP and reciprocal data can be taken. It is more time consuming, but best suited for monitoring. By using CRP, one can easily cover several kilometres per day. In marine environments, this technique is often used in relatively calm estuaries and bays (tidal range mainly below 2 m), which are typically shallow, the maximum water depth of these surveys is mostly less than 3 to 4 m.

Most of the studies found in literature were carried out on the Eastern coastline of the United States (US). The US Geological Survey (USGS) acquired CRP data in e.g. Biscayne Bay (Swarzenski et al., 2004), Neuse River Bay (Cross et al., 2006), Florida Bay (Swarzenski et al., 2009), Manhasset Bay and Northport Harbor (Cross et al., 2012), and Great South Bay (Cross et al., 2013). These are sometimes combined with Radon-222 (e.g. Swarzenski et al. 2004 ; 2009), MER (e.g. Swarzenski and Izbicki, 2009), seismics (e.g. Russoniello et al., 2013 ; Cross et al., 2014), or EM logs in temporary boreholes (e.g. Krantz et al., 2004). There are more illustrations from around the world. For example, Day-Lewis et al. (2006) used CRP to delineate zones of possible SGD in Jobos Bay (Puerto Rico). And the pathways of SGD in a fringing reef (Santiago Island, Philippines) have been studied using CRP, combined with Radon-222 and salinity measurements (Cardenas et al., 2010 ; Cantarero et al., 2019).

Most of the geophysical studies identified above do not bridge the gap between the land and marine realm. Offshore and onshore surveys are rather performed separately, especially if conditions are difficult, e.g. strong tidal and wave activity. Additionally, the spatial and temporal variability of SGD make it more challenging. Onshore surveys alone are generally not sufficient to image the full extent of the SGD zone, while offshore surveys miss the necessary connections with onshore freshwater aquifers. Similarly, while FDEM surveys allow for faster mapping of the salinity than resistivity methods, they do not bring sufficient information on the vertical distribution of salinity.

In this paper, we combine for the first time ERT, CRP, and FDEM. The objective of the survey is to qualitatively map the lateral and vertical distribution of salt and freshwater and identify the SGD zone underneath the near-shore continental shelf, intertidal zone, upper beach, and dunes, at ‘De Westhoek’ nature reserve, Belgium. ERT and CRP provide changes of the



subsurface resistivity in 2D cross-sections, while FDEM mapping provides additional information on lateral variations in the intertidal zone between parallel cross-sections. The combination of CRP during high tide and land ERT collected at low tide ensures that SGD and SI can be accurately imaged at the limit of the low water line. Our case study demonstrates that only a combination of the proposed methods allows to fully characterize the discharge zone in the target area. It also shows that CRP data can directly provide reliable identification of the presence of fresher water, even in very dynamic environments, and that FDEM monitoring can be used to quickly assess seasonal variations in SGD.

## 2 Study area

The study site is located in the most western part of the 65 km long sandy coastline of Belgium, which is delimited by the North Sea in the North and a SW-NE oriented, semi-continuous dune belt in the South, which varies in width. These dunes are part of a long, narrow dune strip that runs from Calais (France) to Northern Denmark. The Belgian coastal dune belt is around 2 km wide at ‘De Westhoek’ – an extensive Flemish nature reserve and European Natura 2000 area – which is located between the Belgian-French border and the city of De Panne (Figure 1). A groundwater extraction site is located in the dunes, exploited by Intercommunale Waterleidingsmaatschappij van Veurne-Ambacht (IWVA). Potable groundwater has been pumped there since 1967.

A low-lying polder area borders the dunes in the South. The shore in the North is tidal dominated (semi-diurnal), with a tidal range of over 5 m at spring tide and approximately 3 m at neap tide. The beach is relatively flat with an average slope of 1.1% (Lebbe, 1981). The shore morphology, tidal range, and permeability of the phreatic aquifer determine the presence of a saltwater lens under the shore – salt water can infiltrate on the back shore during high and spring tide and discharges on the fore shore and/or seabed (Vandenbohede & Lebbe, 2006a).

The sandy aquifer is around 30 m thick at the shore and up to 50 m in the dunes (due to a recent aeolian sand cover) and bounded by Late Eocene heavy marine clays of the Kortrijk Formation, which are considered impermeable. The aquifer is relatively homogeneous at the Belgian-French border, the upper part is fine medium sand and the lower part more coarse and medium sands. It becomes more heterogeneous towards the East, with the local occurrence of silty fine sand lenses (e.g. Lebbe, 1978, 1999).

Freshwater recharges in the dunes, forming a large freshwater lens underneath. This potable water is of high value in the coastal region, since salt and brackish water is often found at shallow depth (i.e. the beach and polder area) (De Breuck et al., 1974 ; Delsman et al., 2019). Part of this freshwater flows underneath the large saltwater lens present in the intertidal zone, forming a freshwater tongue, discharging into the North Sea around the low water line (Vandenbohede & Lebbe, 2006a).

In the past, the migration of groundwater towards the sea has been observed, at ‘De Westhoek’, by electrical and electromagnetic (EM) well logging in 1980 (Lebbe, 1981, 1999) and temperature measurements (Vandenbohede & Lebbe, 2011). Several hydrogeological and groundwater flow models have been developed showing sensitive parameters and past, present, and future evolution of the freshwater tongue (Lebbe, 1983, 1984, 1999 ; Lebbe & Walraevens, 1988 ; Van Camp & Walraevens, 2004 ; Vandenbohede & Lebbe, 2006a, 2006b ; Vandenbohede et al., 2008). However, these models are 2D cross-



sections and do not account for the lateral variations along the coast line. The latter can be revealed by geophysics. In addition, conditions have changed over the years, since the IWVA started a decrease of the exploitation rate at ‘De Westhoek’ in the 1990s. Nowadays, the pumping rate (approximately  $3.2 \times 10^5 \text{ m}^3$  in 2018) is much smaller compared to the 1980s, when pumping rates were between  $1.5$  and  $2.2 \times 10^6 \text{ m}^3 \text{ yr}^{-1}$ .

## 5 3 Methodology

### 3.1 Electrical resistivity

#### 3.1.1 ERT on land

##### 3.1.1.1 Data acquisition

The ABEM Terrameter LS with 64 electrodes was used for the ERT survey on land. Data acquisition took place on multiple days – 7 March (1 km East of the Belgian-French) and 11 October 2018 (at the border). Measurements started during the lowest tide, allowing to measure a wide zone, with the roll-along technique. Using this method, the Terrameter is placed between electrodes 32 and 33. After measuring, it is shifted by 16 or 32 electrodes while new electrodes are positioned at the end of the profile so that the device is back in the middle of the array to perform new measurements. This procedure can be repeated numerous times, to obtain very long ERT profiles, while maintaining relatively homogeneous lateral sensitivity. Combined with a spacing of 5 m between the electrodes, profiles of up to 625 m long were obtained. The multiple-gradient array configuration was chosen for its relatively fast data acquisition speed, which is critical in tidal-dominated environments, and its good compromise between signal-to-noise ratio and resolution (e.g. Dahlin & Zhou, 2006).

#### 3.1.2 Marine CRP

##### 3.1.2.1 Data acquisition

For the marine survey, direct-current CRP is preferred over MER mode (in which electrodes are buried or rest on the sea bottom), since data collection is easier and faster. The use of CRP in a very dynamic environment, such as the North Sea (semi-diurnal tides - tidal range between approximately 3 and 5.3 m - and often relatively strong waves), is not common. Measurements were only performed under relatively calm weather conditions, maximum wave height around 1 m and wind speed maximal 4 bft. CRP is performed near-shore, both during high and low tide to improve the resolution offshore, since the seawater layer is thinner in the latter condition.

Water-borne data was collected at high tide during a single day in 2018 (30 May). The Syscal Pro Deep Marine (IRIS Instruments) was used, combined with a 195 m long floating streamer of 13 graphite takeouts – 2 fixed current electrodes and 11 potential electrodes – spaced at a 15 m interval. Using a reciprocal Wenner-Schlumberger configuration, with the current electrodes in the middle of the set-up, simultaneous collection of 10 resistivity data points was obtained for each current transmission (of 35 to 37 A). The streamer is towed at a relatively constant speed (around  $3.5 \text{ km h}^{-1}$ ) by a small rigid inflatable



boat of the Flanders Marine Institute (VLIZ) collecting data continuously. In order to correct for the influence of the highly conductive seawater layer on the signal, a Garmin GPSMAP 188 Sounder system was directly connected to the Syscal unit (obtaining coordinates and water depth) and seawater conductivity was separately recorded using a CTD diver.

An additional marine survey was carried out on 22 May 2019, allowing to measure during low tide in front of ‘De Westhoek’.

5 Again, the Syscal was used with the same set-up, but with a cable of 130 m. The 13 electrodes were spaced at 10 m, allowing a better resolution yet sufficient penetration in the seabed.

### 3.1.2.2 Pre-processing

In a first step, the raw marine data was checked showing the general trend in apparent resistivity. For the perpendicular high tide profiles, e.g.  $K0_{HT}$  (Figure 2), an increase in resistivity is observed towards the beach. This is not only caused by the decreasing thickness of the seawater layer – since other perpendicular CRP profiles (made at Wenduine where possibly no or much less fresh SGD occurs, Figure 2) barely show this trend towards the land – but mainly due to the outflow of fresh or brackish groundwater. The raw data also displays two bad acquisition channels ( $\rho_6$  and  $\rho_7$ , Figure 2) in all marine profiles (2018) caused by one damaged electrode. These channels were removed from the datasets.

15 The bathymetry was filtered to remove the noise effect caused by the waves, by averaging the data. Also, the echosounder measurements of 2018 comprise multiples. These were, therefore, calibrated with the known shore topography.

### 3.1.3 Processing

Both marine and land ERT data were inversely modeled using the RES2DINVx32 ver. 3.71.118 software. For marine data, potentials are continuously measured which prevents the estimation of the error through stacking or reciprocal measurements. For land ERT, reciprocals could not be collected because of time constraints related to the rising tide. The repeatability error was low, indicating data of good quality. The water layer was included in the CRP data, using the measured seawater conductivity (approximately  $5\,080\text{ mS m}^{-1}$ ) and bathymetry (Loke, 2011). Note that the conductivity of the water layer is introduced as a soft constraint and is not fixed during the inversion. This option was used to prevent the creation of artefacts of inversion as can occur when (potentially erroneous) strong constraints are introduced (Henderson et al., 2010; Caterina et al., 2014).

25 Bad data points were filtered after a first inversion based on the root mean square error ( $E_{RMS} > 100\%$ ). A robust inversion was carried out, using the floating electrodes survey option for the marine profiles. Given the absence of robust error estimates, we relied on the convergence criterion to stop the inversion process (decrease of  $E_{RMS}$  lower than 0.1 % between two iterations). Extended models were obtained of which the absolute errors lie below 2.8 %.

30 The resolution of ERT profiles quickly decreases with depth. This is particularly true for marine profiles as a large portion of the current directly flows in the water layer. The inversion of marine data is thus subject to large uncertainty, especially, the quantitative interpretation of inversion results might be difficult (Day-Lewis et al., 2006). In our case, we are mostly interested in the relative variation of resistivity indicating the presence of fresher water. To obtain information on how much the model



is influenced by the inversion parameters (bathymetry, starting model, etc.) and if reliable resistivity variations are mapped, we propose an approach based on the two-sided difference developed by Oldenburg and Li (1999) for estimating the depth of investigation (DOI). Two additional inversions are carried out using the same dataset, but with 0.1 and 10 times the reference resistivity as a reference model (e.g. the original reference resistivities are 4.926 for profile K1, 1.096 for K1<sub>LT</sub>, and 1.263 for K1<sub>HT</sub>). We assume that we can make a robust qualitative interpretation of the inversion model, when all three models show similar resistivity patterns and are more careful in the evaluation if the models do not agree on the resistivity of certain zones. Although a threshold between 0.1 and 0.2 on the DOI value is often used to delimit reliable zones of the image, this choice is subjective (Caterina et al., 2013). In addition, the DOI is directly sensitive to the absolute value of resistivity and can thus yield high value even for consistently resistive or conductive structures. Therefore, we do not interpret the DOI value itself but interpret it qualitatively with the three respective inversions. For marine data, the DOI is especially influenced by the thickness of the seawater layer (bathymetry), which has a large effect on the calculated value.

### 3.2 Electromagnetic

#### 3.2.1 Data acquisition

Two different FDEM devices were used at 'De Westhoek'. Both have a short acquisition time and are relatively easy to use in the intertidal zone. The DUALEM-421S has the advantage of a larger investigation depth compared to the CMD-MiniExplorer, which only gives information in the upper 2 m.

The CMD-MiniExplorer (GF Instruments, s.r.o., Czech Republic) is a portable multi-depth FDEM device which measures apparent electrical conductivities ( $\text{mS m}^{-1}$ ). It was used for mapping on 23 February 2018. The unit is relatively small and, therefore, easy to use. The entire device is operated by one person, who carries the 1.62 m long probe together with a Trimble GPS (Trimble Navigation Ltd., Sunnyvale, California, USA). The system operates at 30 000 Hz and contains three different receiver coils (dipole distances of 0.32 m (CMD1), 0.71 m (CMD2), and 1.18 m (CMD3)), horizontal coplanar (HCP) configuration was used, giving a cumulative sensitivity of respectively 0.5 m, 1.0 m, and 1.8 m under LIN (Callegary et al., 2007).

Multiple-coil FDEM data were recorded using a DUALEM-421S instrument (DUALEM Inc., Milton, Canada) mounted on a quad on 27 and 28 September 2018, after a very warm and dry summer. The device worked in HCP mode, which resulted in three HCP coil configurations with a coil spacing of 1 (HCP1), 2 (HCP2) and 4 m (HCP4), and three perpendicular (PRP) coil configurations with a coil spacing of 1.1 (PRP1), 2.1 (PRP2) and 4.1 m (PRP4). The instrument's operating frequency was 9 000 Hz and elevation above the ground was 0.195 m. The sampling frequency was 8 Hz at an acquisition speed of approximately  $8 \text{ km h}^{-1}$ , which resulted in a sample (approximately) every 0.25 m. Survey lines were repeated in parallel lines at a spacing of approximately 5.5 m. Geographic coordinates were logged using a Trimble R10 (Trimble Navigation Ltd., Sunnyvale, California, USA) GNSS system.



### 3.2.2 Processing

Basic processing of the DUALEM measurements was done following Delefortrie et al. (2014b ; 2015). The linear relation between the quadrature-phase (QP) component of the electromagnetic field and the LIN ECa (McNeill, 1980) – used in most commercially available FDEM equipment – is not valid in highly conductive environments, as it generally underestimates electrical conductivity. Different from most studies, we convert the LIN ECa data to robust ECa (rECa), making a qualitative interpretation of the FDEM data, acquired in highly conductive environment, possible. We follow the non-linear approach of Hanssens et al. (2019), in which rECa ( $\text{mS m}^{-1}$ ) data are calculated from the QP data to accurately estimate ECa at higher induction numbers (Figure 3). Ultimately, the data were interpolated to a 2 by 2 m grid, via natural neighbour interpolation.

## 4 Results and discussion

10 Due to measurement errors, resolution and inversion constraints it is impossible to deduce the true total dissolved solids (TDS) without a specific calibration of geophysical measurements based on ground truth data. Therefore, we focus on a semi-quantitative interpretation based on relative variations in resistivity. We distinguish three main water quality classes to interpret the geophysical data in the specific study area, using Archie's law (Archie, 1942), the water quality classes of De Moor and De Breuck (1969), and a formation factor of 3.2 (Lebbe, 1981). In the following, we will use a unique colour scale to describe the results in all figures (except in Figure 6): freshwater occurs in zones with a resistivity higher than approximately 20  $\Omega\text{m}$  (blue), salt water has a resistivity lower than roughly 2.5  $\Omega\text{m}$  (red), and brackish water leads to intermediate resistivities (light brown to light blue). In the case of the Belgian coast, the strong tides play a role, increasing the portion of RSGD in SGD, and making the distinction - based on resistivity/conductivity - between submarine discharge and the seawater more difficult. The discharge zone will thus not be necessarily characterized by freshwater but rather by brackish water.

20 In the following paragraphs, we present the data as they were collected on the field. In this way, our natural reasoning in the investigation of SGD and the incremental understanding of the discharge zone are illustrated, while highlighting the complementarity between the different geophysical methods.

We started our investigation with the CMD-MiniExplorer mapping at the location of one of the profiles (K1, located at 1 km East from the French-Belgian border) of Lebbe (1981). Previous studies had shown the presence of freshwater under the saltwater lens but could not identify the discharge zone. The CMD-MiniExplorer mapping (Figure 3, right, and Figure 7, A.) identifies the presence of SGD close to the low water line, at K1, indicated by a decrease in the electrical conductivity. The FDEM data clearly demonstrates a zone which is over 100 m wide. The outflowing water is very brackish to moderately salt, the conductivity is roughly between 350 and 650  $\text{mS m}^{-1}$ , due to a mixture of discharging fresh groundwater and seawater that infiltrated on the beach during high tide.

30 Interpreted on its own, this variation of resistivity could be related to lithological heterogeneities or the presence of near-surface features. Therefore, we carried out a long land ERT profile (635 m, Figure 4, K1) covering the entire zone between the low water line and the dune area. At the right side of the section, we identify the freshwater aquifer located in the dune area.



The brackish water observed at -10 mTAW corresponds to remnants of seawater infiltration during the flooding of an artificial tidal inlet, which started in 2004 and ended a few years ago. The downward movement of the denser seawater is hindered by the presence of a clay lens (Vandenbohede et al., 2008; Hermans et al., 2012). Along this profile, there is a large saltwater lens on the beach with a thickness of around 15 m. Underneath, freshwater is flowing from the dunes towards the North Sea. The  
5 freshwater mixes with the recharging seawater, leading to the discharge of salt to brackish water during low tide on the lower beach. This is clearly visible at the left side of the land profile, where fresher water is seen near the surface, which corresponds to the zone identified by EM measurements.

The identified saltwater lens (at K1) is similar in size as observed in 1980, based on well loggings on the beach (Lebbe, 1981). However, the lens does no longer extend to the sea, since the freshwater tongue reaches the surface nowadays on the lower  
10 beach. This is probably an effect of the decreasing pumping trend of the IWVA exploitation site: the rate is now over 4.5 times lower compared to 1980, which has subsequently strengthened the groundwater discharge.

In the centre of the profile, the thickness of the salt water lens is maximum (15 m), while the bottom boundary of the aquifer (thick clay layer) is located between -25 and -30 mTAW. The groundwater appears to be brackish in this zone. This is likely a result from the smoothness constraint inversion combined with the lower resolution at depth as the more resistive freshwater  
15 is bounded by two conductive layers, leading to a lower inverted resistivity.

The profile was extended by a marine profile collected at high tide, with an overlapping zone of about 230 m (Figure 4, K1<sub>HT</sub>). The latter confirms the presence of brackish water below the saltwater. It indicates that the discharge zone is not limited to the low water line, but that it could extend towards the sea. At 200 m in front of the low water mark, weakly salt water is migrating towards the seabed (light red colour). Further offshore, a marine profile, collected at low tide (Figure 5, K1<sub>LT</sub>), confirms that  
20 brackish pore water can be seen up to at least 550 m from the low water line. It is mixed with seawater which recirculates in the seabed, making it impossible to visualize SGD at the seabed using resistivity measurements, but the brackish groundwater is clearly pushed upwards.

Note that the resolution of the marine profile at high tide is significantly lower, since: it has a thicker seawater layer above the sea bottom, the portion of RSGD in the discharge increases from low to high tide, it is collected in other dynamic conditions  
25 (significant groundwater discharge might only occur at low tide, since the hydraulic gradient between land and sea is larger compared to the high tide), and the electrodes of the streamer were spaced closer during the low tide survey.

There is a similar situation 1 km to the West, at the Belgian-French border (Figure 4, K0), where freshwater moves underneath a saltwater lens from the dunes towards the sea. Nevertheless, a striking difference on this profile is the absence of freshwater flowing upwards and discharging on the lower beach. Indeed, the saltwater lens, although becoming thinner towards the low water line, remains continuous. At the left side of the profile, the underlying water is identified as fresh whereas it seems more brackish towards the dunes. This is probably related to the higher resolution at depth when the conductive salt layer is thinner  
30 and not due to an actual variation in salinity. On this profile, the clay layer underlying the coastal aquifer is also detected around -35 mTAW.



The shape and thickness of the saltwater lens at this location have not changed much since 1980 (Lebbe, 1981). The lens becomes thinner towards the low water line, but there is no discharge on the lower beach, since SGD is located below this level. K0 is located furthest from the IWVA site and no large extractions are known to occur on the French side of the border. The resistivity profiles at the border give the natural distribution of salt and freshwater, meaning with the least anthropogenic effect in the study site. As a consequence, the pore water is more resistive underneath the beach and further offshore compared to K1. At high tide, outflowing groundwater is overlain by a thin layer in which pore water is salt (Figure 4, K0<sub>HT</sub>). But the underlying brackish pore water moves upward approximately 250 m in front of the low water line. The brackish lens extends further offshore (Figure 5, K0<sub>LT</sub>), moving upward, and is mixed with salt water. SGD does not reach as far offshore compared to K1<sub>LT</sub> (Figure 5), perhaps due to different local hydrogeological and geological conditions.

Note that the presence of fresher water is clearly visible on the raw data (Figure 2). Possible zones of SGD can be identified without needing to invert the data. CRP can therefore be used as a fast exploration technique to locate zones of brackish/fresh pore water. Using this technique one can easily survey multiple kilometres per day along the coastlines to detect the most vulnerable sites in terms of nutrient/contaminant leakage to the aquatic environment and loss of freshwater.

To acquire information on the variation parallel to the beach, CRP profiles were obtained during high tide (Figure 6). On the lower beach, the pore water resistivity increases from K1 towards K0 (Figure 6, M1). This trend is partly due to the thinner saltwater lens in the West, which increases the resolution of the inversion model. But also due to a higher groundwater flux, since part of the profile (close to the middle) has a thicker lens compared to the zone around K1, while the water underneath K1 is less fresh. Also closer to the low water line, resistivity increases from K1 to K0 (Figure 6, M2). Towards the East, a more resistive body is seen (Figure 6, M3), visible on the raw data, while in the far east of the profile (in front of the IWVA site), the resistivity is much lower compared to K1. The higher resistivity between the IWVA and K1 can have multiple reasons, which need further investigation. The thickness of the overlying saltwater lens can have an effect, as well as the dike between the beach and dunes, which is closer to the sea in that zone. Local hydrogeological heterogeneities can have an influence, too. Maintaining the cable exactly parallel to the beach was also challenging, some measurement distortions are thus also possible. To confirm the lateral variations in SGD along this part of the coast, another profile was collected further East (Figure 5, K1.5<sub>LT</sub>). Discharge seems stronger on K1<sub>LT</sub> compared to K1.5<sub>LT</sub>, since it extends further offshore (Figure 5). This observation is logical, K1.5<sub>LT</sub> is closer to the IWVA extraction site and, so, more affected by the water extraction reducing groundwater discharge. However, this should be further examined.

To further investigate lateral variation between the K0 and K1 profiles, the intertidal zone was mapped with EM (DUALEM) at the vicinity of the low water line, where discharge was observed in the zone around K1 (Figure 3 and Figure 4, K1). This map clearly demonstrates a northward shift of the zone of discharge from K1 towards K0 (Figure 7). From approximately 300 m East of the border, the discharge zone is no longer visible from the EM data since the discharge is located below the low water line. The DUALEM was dragged on the beach in a sled, making the quality of the data higher compared to the MiniExplorer, which was carried by hand, making it difficult to maintain a constant height above the surface during mapping.



The water conductivity, obtained with the DUALEM-421S, in the discharge zone corresponds to a brackish water type, confirming the mixing of freshwater with recirculated seawater.

The MiniExplorer and DUALEM data were collected in two different seasons, respectively the end of Winter and beginning of Autumn. The discharge around K1 is different in February (MiniExplorer) compared to October (DUALEM-421S) (Figure 7). During the former, the outflow of groundwater is clearly seen around K1 with CMD3. Whereas in October, a large zone of salty-brackish discharge is well visible using HCP4-, but only seen as individual spots of slightly lower conductivity with HCP1 and PRP4. **This indicates that fresh SGD is stronger in Winter than Autumn.** This is due to the lower precipitation and higher evapo(transpiration) in Summer, leading to smaller groundwater fluxes. **In 2018, Summer was particularly dry in Belgium.**

To validate the results of the ERT and CRP inversion, we use the two-sided difference approach, additionally computing the inversion for two different reference models. For land profiles, e.g. K1 (Figure 8, A), all three inversions look almost perfectly similar, indicating that observed structures are qualitatively contained in the data. For profiles at high tide, e.g. K1<sub>HT</sub> (Figure 8, C), lateral variations are also similar in the different inversion models, identifying fresher water towards the beach. However, small variations are observed vertically around the sea bottom, corresponding to DOI values above 0.2, showing that the inversion is particularly sensitive to the bathymetry and the presence of the seawater layer. In this case, a high conductivity reference model will force some more resistive features to appear closer to the sea bottom. As a consequence, the discharge zone seems closer to the sea bottom. Whether this is actually the case or not cannot be elucidated from our measurements. For low-tide profiles, e.g. K1<sub>LT</sub> (Figure 8, B), fewer differences are observed compared to those taken during high tide. In summary, all profile types, although with different intrinsic resolutions, are sensitive enough to characterize the general salinity distribution in the studied zone.

## 5 Conclusions

In this contribution, we propose an innovative combination of land and marine ERT together with FDEM mapping to characterize fresh groundwater discharge. Electrical and electromagnetic methods constitute practical tools in the investigation of SGD in coastal environments. The very high spatial lateral resolution of FDEM combined with the vertical resolution of ERT allows to interpret the presence of fresher water in 3D, while minimizing the field effort and the acquisition time. By continuing ERT profiles seaward using CRP, the surveyed area can be extended offshore to identify discharge zones located below the low water line. While resistivity tomography is used to obtain a general 2D or pseudo-3D model of the salt and freshwater distribution on land, in the intertidal zone, and offshore, FDEM mapping provides information on lateral variations. Since the data acquisition is rapid and easy-to-use, this is perfectly suited for the investigation of the intertidal zone and to fill the gap between ERT profiles that take longer to acquire.

As standard output of commercially available (LIN) FDEM instrumentation systematically underestimates E<sub>Ca</sub> values in highly conductive environments, the technique has, to our knowledge, only rarely been used in the intertidal zone. However,



limitations imposed by high conductive environments can be overcome through more robust interpretation of collected QP data (e.g. Hanssens et al., 2019). This further extends the potential of FDEM to characterize SGD and SI in littoral zones.

We demonstrate the ability of the proposed methodology to characterize freshwater discharge occurring at 'De Westhoek' in the western Belgian coastal plain. In this area, SGD is present both below sea level and in the intertidal zone. Land ERT profiles clearly identify the saltwater lens, underlain by freshwater, and originating from the infiltration of seawater on the low slope shore and discharging on the lower beach. CRP surveys further image the presence of brackish pore water and SGD offshore. FDEM mapping in the intertidal zone allows to characterize lateral variations in the discharge zone and to locate where it becomes submarine.

To our knowledge, this constitutes the first comprehensive imaging of both the saltwater lens under the beach and the shifting of SGD seawards using geophysical techniques. The discharge is best-visible during low tide, since the groundwater flux is higher compared to high tide and there is less recirculating seawater. Low-tide conditions also allow to maximize the resolution of both land and marine ERT, while enabling the acquisition of FDEM data in the intertidal zone. The groundwater discharge has a seasonal variability, SGD is higher at the end of Winter compared to the beginning of Autumn, since a warm and dry Summer precedes the latter.

In the future, we plan to use the geophysical data and more classical hydrogeological data to calibrate a 3D groundwater model of the zone in order to quantify SGD.

## 6 Acknowledgement

The CRP surveys were funded by the VLIZ *Brilliant Marine Research Idea grant* (2018) and the FWO Research credit (FWO1505219N). We want to thank the VLIZ for their logistical support in the marine surveys and Liège University for lending the land ERT equipment. The authors would also like to acknowledge Josue Chishugi, Nicolas Compaire, Tim Deckmyn, Anja Derycke, Gaël Dumont, Hadrien Michel, Melissa Prieto, Mizanur Rahman Sarker, Robin Thibaut, Bart Van Impe, Valentijn Van Parys, Jan Vermaut, & Nele Vlamynck for their help with the field work.

## References

Archie, G. E.: The electrical resistivity log as an aid in determining some reservoir characteristics. *Transactions of the AIME*, 146 (1), 54-62, <https://doi.org/10.2118/942054-G>, 1942.

Bates, C.R. and Bates, M.R.: Palaeogeographic Reconstruction in the Transitions Zone: The Role of Geophysical Forward Modelling in Ground Investigation Surveys, *Archaeological Prospection*, 23(4), 311-323, <https://doi.org/10.1002/arp.1546>, 2016.

Bonsall, J. and Dowd, M.: Emerging from the waves: a late Bronze Age intertidal saltwater *fulacht fia* at Coney Island, Co. Sligo, *The Journal of Irish Archaeology*, 24, 79-95, 2015.



- Burnett, W.C., and Dulaiova, H.: Estimating the dynamics of groundwater input into the coastal zone via continuous radon-222 measurements, *Journal of Environmental Radioactivity*, 69(1-2), 21-35, [https://doi.org/10.1016/S0265-931X\(03\)00084-5](https://doi.org/10.1016/S0265-931X(03)00084-5), 2003.
- Burnett, B., Bokuniewicz, H., Huettel, M., Moore, W.S., and Taniguchi, M.: Groundwater and pore water inputs to the coastal zone, *Biogeochemistry*, 66(1-2), 3-33, <https://doi.org/10.1023/B:BIOG.0000006066.21240.53>, 2003.
- 5 Burnett, W.C., Aggarwal, P.K., Aureli, A., Bokuniewicz, H., Cable, J.E., Charette, M.A., Kontar, E., Krupa, S., Kulkarni, K.M., Loveless, A., Moore, W.S., Oberdorfer, J.A., Oliveira, J., Ozyurt, N., Povinec, P., Privitera, A.M.G., Rajar, R., Ramessur, R.T., Scholten, J., Stieglitz, T., Taniguchi, M., and Turner, J.V.: Quantifying submarine groundwater discharge in the coastal zone via multiple methods, *Science of the Total Environment*, 367(2-3), 498-543, <https://doi.org/10.1016/j.scitotenv.2006.05.009>, 2006.
- 10 Callegary, J.B., Ferré, T.P.A., and Groom, R.W.: Vertical Spatial Sensitivity and Exploration Depth of Low-Induction-Number Electromagnetic-Induction Instruments, *Vadose Zone Journal*, 6(1), 158-167, <https://doi.org/10.2136/vzj2006.0120>, 2007.
- Cantarero, D.L.M., Blanco, A., Cardenas, M.B., Nadaoka, K., and Siringan, F.P.: Offshore Submarine Groundwater Discharge at a Coral Reef Front Controlled by Faults, *Geochemistry, Geophysics, Geosystems*, 20(7), <https://doi.org/10.1029/2019GC008310>, 2019.
- 15 Cardenas, M.B., Zamora, P.B., Siringan, F.P., Lapus, M.R., Rodolfo, R.S., Jacinto, G.S., Diego-McGlone, M.L.S., Villanoy, C.L., Cabrera, O., and Senal, M.I.: Linking regional sources and pathways for submarine groundwater discharge at a reef by electrical resistivity tomography, 222Rn, and salinity measurements, *Geophysical Research Letters*, 37(6), L16401, <https://doi.org/10.1029/2010GL044066>, 2010.
- 20 Caterina, D., Beaujean, J., Robert, T., and Nguyen, F.: A comparison study of different image appraisal tools for electrical resistivity tomography, *Near Surface Geophysics*, 11, 639–657, <https://doi.org/10.3997/1873-0604.2013022>, 2013.
- Caterina, D., Hermans, T., and Nguyen, F.: Case studies of incorporation of prior information in electrical resistivity tomography: comparison of different approaches, *Near Surface Geophysics*, 12(4), 451-465, <https://doi.org/10.3997/1873-0604.2013070>, 2014.
- 25 Colman, J.A., Masterson, J.P., Pabich, W.J., and Walter, D.A.: Effects of Aquifer Travel Time on Nitrogen Transport to a Coastal Embayment, *Ground Water*, 42(7), 1069-1078, <https://doi.org/10.1111/j.1745-6584.2004.tb02644.x>, 2004.
- Cross, V.A., Bratton, J.F., Bergeron, E.M., Meunier, J.K., Crusius, J., and Koopmans, D.: Continuous resistivity profiling data from the upper Neuse River Estuary, North Carolina, 2004-2005, U.S. Geological Survey, Virginia, Open-File Report 2005-1306, 2006.
- 30 Cross, V.A., Bratton, J.F., Crusius, J., Kroeger, K.D., and Worley, C.R.: Continuous resistivity profiling data from Northport Harbor and Manhasset Bay, Long Island, New York, U.S. Geological Survey, Virginia, Open-File Report 2011-1041, <https://doi.org/10.3133/ofr20111041>, 2012.
- Cross, V.A., Bratton, J.F., Kroeger, K.D., Crusius, J., and Worley, C.R.: Continuous resistivity profiling data from Great South Bay, Long Island, New York, U.S. Geological Survey, Virginia, Open-File Report 2011-1040, 2013.



- Cross, V.A., Bratton, J.F., Michael, H.A., Kroeger, K.D., Green, A., and Bergeron, E.M.: Continuous resistivity profiling and seismic-reflection data collected in April 2010 from Indian River Bay, Delaware, U.S. Geological Survey, Virginia, Open-File Report 2011-1039, <https://doi.org/10.3133/ofr20111039>, 2014.
- Dahlin, T. and Zhou, B.: Multiple-gradient array measurements for multichannel 2D resistivity imaging, *Near Surface Geophysics*, 4(2), 113-123, <https://doi.org/10.3997/1873-0604.2005037>, 2006.
- Davies, G., Huang, J., Monteiro Santos, F.A., and Triantafylis, J.: Modeling Coastal Salinity in Quasi 2D and 3D Using a DUALEM - 421 and Inversion Software, *Groundwater*, 53(3), 424-431, <https://doi.org/10.1111/gwat.12231>, 2015.
- Day-Lewis, F.D., White, E.A., Johnson, D., and Lane, J.W. Jr.: Continuous resistivity profiling to delineate submarine groundwater discharge—examples and limitations, *THE LEADING EDGE*, June, 724-728, <https://doi.org/10.1190/1.2210056>, 2006.
- De Moor, G. and De Breuck, W.: De freatische waters in het Oostelijk Kustgebied en de Vlaamse Vallei, *Natuurlijk Tijdschrift*, 51, 3-68, 1969.
- De Breuck, W., De Moor, G., Maréchal, R., and Tavernier, R. (1974). Diepte van het grensvlak tussen zoet en zout water in de freatische laag van het Belgische kustgebied (1963-1773). Verziltingskaart. Militair Geografisch Instituut, Brussel.
- de Franco, E., Biella, G., Tosi, L., Teatini, P., Lozej, A., Chiozzotto, B., Giada, M., Rizzetto, F., Claude, C., Mayer, A., Bassan, V., and Gasparetto-Stori, G.: Monitoring the saltwater intrusion by time lapse electrical resistivity tomography: The Chioggia test site (Venice Lagoon, Italy), *Journal of Applied Geophysics*, 69(3-4), 117-130, <https://doi.org/10.1016/j.jappgeo.2009.08.004>, 2009.
- Delefortrie, S., Saey, T., Van De Vijver, E., De Smedt, P., Missiaen, T., Demerre, I., and Van Meirvenne, M.: Frequency domain electromagnetic induction survey in the intertidal zone: Limitations of low-induction-number and depth exploration, *Journal of Applied Geophysics*, 100, 14-22, <http://doi.org/10.1016/j.jappgeo.2013.10.005>, 2014a.
- Delefortrie, S., De Smedt, P., Saey, T., Van De Vijver, E., and Van Meirvenne, M.: An efficient calibration procedure for correction of drift in EMI survey data, *Journal of Applied Geophysics*, 110, 115-125, <https://doi.org/10.1016/j.jappgeo.2014.09.004>, 2014b.
- Delefortrie, S., Saey, T., De Pue, J., Van De Vijver, E., De Smedt, P., Van Meirvenne, M.: Evaluating corrections for a horizontal offset between sensor and position data for surveys on land, *Precision Agriculture*, 17(3), 349-364, <https://doi.org/10.1007/s11119-015-9423-8>, 2015.
- Delsman, J., van Baaren, E., Vermaas, T., Karaoulis, M., Bootsma, H., de Louw, P., Pauw, P., Oude Essink, G., Dabekaussen, W., Van Camp, M., Walraevens, K., Vandenbohede, A., Teilmann, R., and Thofte, S.: TOPSOIL Airborne EM katerering van zoet en zout grondwater in Vlaanderen (FRESHM Vlaanderen). Vlaamse Milieumaatschappij, 111 pp., 2019.
- Dimova, N.T., Swarzenski, P.W., Dulaiova, H., and Glenn, C.R.: Utilizing multichannel electrical resistivity methods to examine the dynamics of the fresh water–seawater interface in two Hawaiian groundwater systems, *Journal of Geophysical Research*, 117, C02012, <https://doi.org/10.1029/2011JC007509>, 2012.



- Evans, R.L., Law, L.K., St. Louis, B., Cheesman, D., and Sananikone, K.: The shallow porosity structure of the Eel shelf, northern California: results of a towed electromagnetic survey, *Marine Geology*, 154(1-4), 211-226, [https://doi.org/10.1016/S0025-3227\(98\)00114-5](https://doi.org/10.1016/S0025-3227(98)00114-5), 1999.
- Francés, A.P., Ramalho, E.C., Fernandes, J., Groen, M., Hugman, R., Khalil, M.A., De Plaen, J., and Monteiro Santos, F.A.: Contribution of hydrogeophysics to the hydrogeological conceptual model of the Albufeira-Ribeira de Quarteira coastal aquifer in Algarve, Portugal, *Hydrogeological Journal*, 23(7), 1553-1572, <http://doi.org/10.1007/s10040-015-1282-x>, 2015.
- Goebel, M., Pidlisecky, A., and Knight, R.: Resistivity imaging reveals complex pattern of saltwater intrusion along Monterey coast, *Journal of Hydrology*, 551, 746-755, <https://doi.org/10.1016/j.jhydrol.2017.02.037>, 2017.
- Goebel, M., Knight, R., and Halkjær, M.: Mapping saltwater intrusion with an airborne electromagnetic method in the offshore coastal environment, Monterey Bay, California, *Journal of Hydrology: Regional Studies*, 23, 100602, <https://doi.org/10.1016/j.ejrh.2019.100602>, 2019.
- Goldman, M., Gilad, D., Ronen, A., and Melloul, A.: Mapping of seawater intrusion into the coastal aquifer of Israel by the time domain electromagnetic method, *Ge exploration*, 28(2), 153-174, [https://doi.org/10.1016/0016-7142\(91\)90046-F](https://doi.org/10.1016/0016-7142(91)90046-F), 1991.
- Goldman, M., Gvirtzman, H., and Hurwitz, S.: Mapping saline groundwater beneath the Sea Galilee and its vicinity using time domain electromagnetic (TDEM) geophysical technique, *Israel Journal of Earth Sciences*, 53(3-4), 187-197, <https://doi.org/10.1560/P1W7-UYDE-WJFW-CVHB>, 2004.
- Greenwood, W.J., Kruse, S., and Swarzenski, P.: Extending Electromagnetic Methods to Map Coastal Pore Water Salinities, *Groundwater*, 44(2), 292-299, <https://doi.org/10.1111/j.1745-6584.2005.00137.x>, 2006.
- Gunn, D.A., Pearson, S.G., Chambers, J.E., Nelder, L.M., Lee, J.R., Beamish, D., Busdy, J.P., Tinsleyn, R.D., and Tinsley, W.H., An evaluation of combined geophysical and geotechnical methods to characterize beach thickness, *Quarterly Journal of Engineering Geology and Hydrogeology*, 39(4), 339-355, <https://doi.org/10.1144/1470-9236/05-038>, 2006.
- Hanssens, D., Defortrie, S., Bobe, C., Hermans, T., and De Smedt, P.: Improving the reliability of soil EC-mapping: Robust apparent electrical conductivity (rECa) estimation in ground-based frequency domain electromagnetics, *Geoderma*, 337, 1155-1163, <https://doi.org/10.1016/j.geoderma.2018.11.030>, 2019.
- Henderson, R.D., Day-Lewis, F.D., Abarca, E., Harvey, C.F., Karam, H.N., Liu, L., and Lane, J.W. Jr.: Marine electrical resistivity imaging of submarine groundwater discharge: sensitivity analysis and application in Waquoit Bay, Massachusetts, USA, *Hydrogeology Journal*, 18(1), 178-185, <https://doi.org/10.1007/s10040-009-0498-z>, 2010.
- Hermans, T., Vandenbohede, A., Lebbe, L., Martin, R., Kemna, A., Beaujean, J., and Nguyen, F.: Imaging artificial salt water infiltration using electrical resistivity tomography constrained by geostatistical data, *Journal of Hydrology*, 438-439, 168-180, <https://doi.org/10.1016/j.jhydrol.2012.03.021>, 2012.
- Hoefel FG and Evans, R.L.: Impact of Low Salinity Porewater on Seafloor Electromagnetic Data: A Means of Detecting Submarine Groundwater Discharge?, *Estuarine, Coastal and Shelf Science*, 52(2), 179-189, <https://doi.org/10.1006/ecss.2000.0718>, 2001.



- Hwang, D.-W., Lee, Y.-W., and Kim, G.: Large submarine groundwater discharge and benthic eutrophication in Bangdu Bay on volcanic Jeju Island, Korea, *Limnology and Oceanography*, 50(5), 1393-1403, <https://doi.org/10.4319/lo.2005.50.5.1393>, 2005.
- Kontar, E.A., and Ozorovich, Y.R.: Geo-electromagnetic survey of the fresh/salt water interface in the coastal southeastern Sicily, *Continental Shelf Research*, 26(7), 843-851, <https://doi.org/10.1016/j.csr.2005.12.012>, 2006.
- Krantz, D.E., Manheim, F.T., Bratton, J.F., and Phelan, D.J.: Hydrogeologic Setting and Ground Water Flow Beneath a Section of Indian River Bay, Delaware, *Groundwater*, 42(7), 1035-1051, <https://doi.org/10.1111/j.1745-6584.2004.tb02642.x>, 2006.
- Lapointe, B.E., Barile, P.J., Littler, M.M., and Littler, D.S.: Macroalgal blooms on southeast Florida coral reefs II. Cross-shelf discrimination of nitrogen sources indicates widespread assimilation of sewage nitrogen, *Harmful Algae*, 4(6), 1103-1122, <https://doi.org/10.1016/j.hal.2005.06.002>, 2005.
- Lebbe, L.: Hydrogeologie van het duingebied ten westen van De Panne, Ph.D. thesis, Ghent University, Belgium, 164pp., 1978.
- Lebbe, L.: The subterranean flow of fresh and salt water underneath the Western Belgian beach, in: *Proceedings of the 7th Salt Water Intrusion Meeting*, Uppsala, Sweden, 193-219, 1981.
- Lebbe, L.: Mathematical model of the evolution of the fresh water lens under the dunes and beach with semi-diurnal tides, *Geologia applicata e idrogeologia*, 18(2), 211-226, 1983.
- Lebbe, L.: Numerische simulatie van grondwaterkwaliteitsproblemen als hulp bij het beheer van de watervoorraden in het Vlaamse kustgebied, *Tijdschrift BECEWA*, 76, 67-88, 1984.
- Lebbe, L.: Parameter identification in fresh-saltwater flow based on borehole resistivities and freshwater head data, *Advances in Water Resources*, 22(8), 791-806, [https://doi.org/10.1016/S0309-1708\(98\)00054-2](https://doi.org/10.1016/S0309-1708(98)00054-2), 1999.
- Lebbe, L. and Walraevens, K.: Hydrogeological SWIM-excursion to the western coastal plain of Belgium, in: *Proceedings of the 10th Salt Water Intrusion Meeting*, Ghent, Belgium, 16-20 May, 359-375, 1988.
- Loke, M. H. : RES2DINV ver. 3.71. Rapid 2-D resistivity & IP inversion using the least squares method, 2011.
- McNeill, J.D: Electromagnetic terrain conductivity measurement at low induction numbers, Technical Note, Geonics, Canada, 15pp., 1980.
- Michael, H.A., Mulligan, A.E., and Harvey, C.F.: Seasonal oscillations in water exchange between aquifers and the coastal ocean, *Nature*, 436, 1145-1148, <https://doi.org/10.1038/nature03935>, 2005.
- Moore, W.S.: The Effect of Submarine Groundwater Discharge on the Ocean, *Annual Review of Marine Science*, 2, 59-88, <https://doi.org/10.1146/annurev-marine-120308-081019>, 2010.
- Obikoya I.B. and Bennell, J.D.: Geophysical Investigation of the Fresh-Saline Water Interface in the Coastal Area of Abergwyngregyn, *Journal of Environmental Protection*, 3(9), 1039-1046, <https://doi.org/10.4236/jep.2012.39121>, 2012.
- Ogilvy, R.D., Meldrum, P.I., Wilkinson, P.B., Chambers, J.E., Sen, M., Pulido-Bosch, A., Gisbert, J., Jorreto, S., Frances, I., and Tsourlos, P.: Automated monitoring of coastal aquifers with electrical resistivity tomography, *Near Surface Geophysics*, 7(5-6), 367-376, <https://doi.org/10.3997/1873-0604.2009027>, 2009.



- Oldenburg, D.W., and Li, Y.: Estimating depth of investigation in dc resistivity and IP surveys, *Geophysics*, 64(2), 403-416, <https://doi.org/10.1190/1.1444545>, 1999.
- Paine, J.: Determining salinization extent, identifying salinity sources, and estimating chloride mass using surface, borehole, and airborne electromagnetic induction methods, *Water Resources Research*, 39(3), 1059, <https://doi.org/10.1029/2001WR000710>, 2003.
- Palacios, A., Ledo, J., Linde, N., Carrera, J., Luquot, L., Bellmund, F., Folch, A., Bosch, D., Del Val, L., Martínez, L., Goyetche, T., Diego-Feliu, M., Garcia-Orellana, J., and Pool, M.: Time-lapse cross hole electrical resistivity tomography (CHERT) for monitoring seawater intrusion dynamics in a Mediterranean aquifer, in: *Proceedings of the 25th Salt Water Intrusion Meeting*, Gdansk, Poland, 17-22 June 2018, 82-83, 2018.
- 10 Pauw, P.S.: The onshore and offshore groundwater salinity distribution between Egmond aan Zee and Castricum aan Zee, Master thesis, Vrije Universiteit Amsterdam, Nederland, 53pp., 2009.
- Russoniello, C.J., Fernandez, C., Bratton, J.F., Banaszak, J.F., Krantz, D.E., Andres, A.S., Konikow, L.F., and Michael, H.A.: Geologic effects on groundwater salinity and discharge into an estuary, *Journal of Hydrology*, 498, 1-12, <https://doi.org/10.1016/j.jhydrol.2013.05.049>, 2013.
- 15 Swarzenski, P.W. and Izbecki, J.A.: Coastal groundwater dynamics off Santa Barbara, California: Combining geochemical tracers, electromagnetic seepmeters, and electrical resistivity, *Estuarine, Coastal and Shelf Science*, 83(1), 77-89, <https://doi.org/10.1016/j.ecss.2009.03.027>, 2009.
- Swarzenski, P.W., Burnett, B., Reich, C., Dulaiova, H., Peterson, R., and Meunier, J.: Novel geophysical and geochemical techniques used to study submarine groundwater discharge in Biscayne Bay, Florida, U.S. Geological Survey, Virginia, Fact Sheet 3117, 2004.
- 20 Swarzenski, P.W., Burnett, W.C., Greenwood, W.J., Herut, B., Peterson, R., Dimova, N., Shalem, Y., Yechieli, Y., and Weinstein, Y.: Combined time - series resistivity and geochemical tracer techniques to examine submarine groundwater discharge at Dor Beach, Israel, *Geophysical Research Letters*, 33(24), L24405, <https://doi.org/10.1029/2006GL028282>, 2006.
- Swarzenski, P.W., Reich, C., and Rudnick, D.: Examining Submarine Ground-Water Discharge into Florida Bay by using 222Rn and Continuous Resistivity Profiling, U.S. Geological Survey, Virginia, Open-File Report 2008-1342, 2009.
- 25 Taniguchi, M., Burnett, W.C., Cable, J.E., and Turner, J.V.: Investigation of submarine groundwater discharge, *Hydrological Processes*, 16(11), 2115-2129, <https://doi.org/10.1002/hyp.1145>, 2002
- Taniguchi, M., Ishitobi, T., Burnett, W.C., and Wattayakorn, G.: Evaluating Ground Water–Sea Water Interactions via Resistivity and Seepage Meters, *Groundwater*, 45(6), 729-735, <https://doi.org/10.1111/j.1745-6584.2007.00343.x>, 2007.
- 30 Van Camp, M. and Walraevens, K.: Direct groundwater discharge to the North Sea. A case study for the Western Belgian coast, in: *Proceedings of the 18th Salt Water Intrusion Meeting*, Cartagena, Spain, 31 May-3 June, 139-150, 2004.
- Vandenbohede, A. and Lebbe, L.: Occurrence of salt water above fresh water in dynamic equilibrium in a coastal groundwater flow system near De Panne, Belgium, *Hydrogeological Journal*, 14(4), 462-472, <https://doi.org/10.1007/s10040-005-0446-5>, 2006a.



- Vandenbohede, A. and Lebbe, L.: Effects of tides on a sloping shore: groundwater dynamics and propagation of the tidal wave, *Hydrogeological Journal*, 15(4), 645-658, <https://doi.org/10.1007/s10040-006-0128-y>, 2006b.
- Vandenbohede, A. and Lebbe, L.: Heat transport in a coastal groundwater flow system near De Panne, Belgium, *Hydrogeology Journal*, 19(6), 1225-1238, <https://doi.org/10.1007/s10040-011-0756-8>, 2011.
- 5 Vandenbohede, A., Luyten, K., and Lebbe, L.: Effects of Global Change on Heterogeneous Coastal Aquifers: A Case Study in Belgium, *Journal of Coastal Research*, 24(2B), 160-170, <https://doi.org/10.2112/05-0447.1>, 2008.
- Viezzoli, A., Tosi, L., Teatini, P., and Silvestri, S.: Surface water–groundwater exchange in transitional coastal environments by airborne electromagnetics: The Venice Lagoon example, *Geophysical Research Letters*, 37(1), L01402, <https://doi.org/10.1029/2009GL041572>, 2010.
- 10 Viezzoli, A., Munday, and Y.L. Cooper: Airborne electromagnetics for groundwater salinity mapping: case studies of coastal and inland salinisation from around the world, *Bollettino di Geofisica Teorica ed Applicata*, 53(4), 581-600, <https://doi.org/10.4430/bgta0067>, 2012.

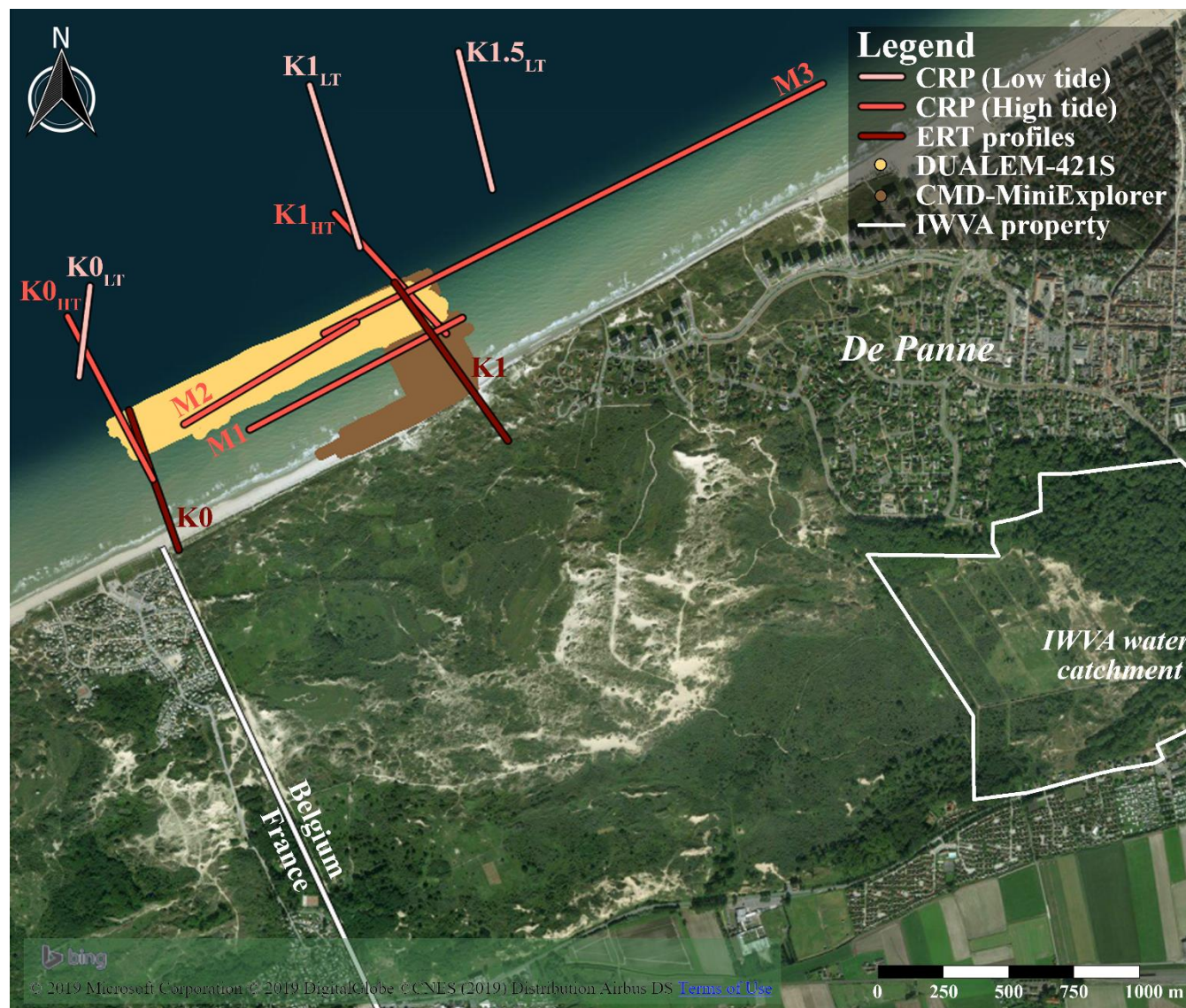


**Figure 1:** The Westhoek study area, between the Belgian-French border and De Panne city. With the location of the ERT, CRP profiles, the zones of FDEM mapping, and the IWVA groundwater extraction site. Copyright: Microsoft Corporation, DigitalGlobe, and CNES, 2019.

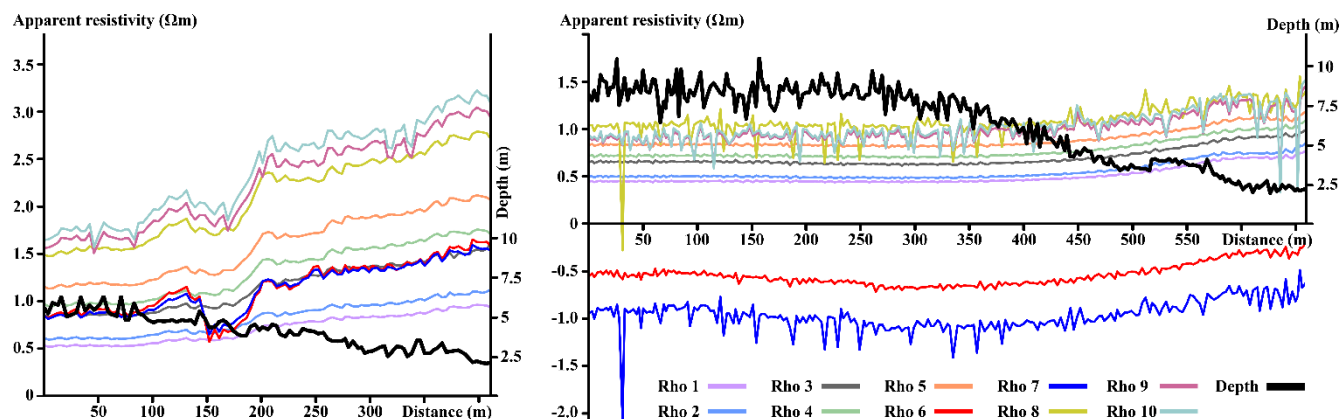


Figure 2: Raw resistivity data plots versus bathymetry. Left: profile K0HT: strong resistivity increase towards the beach, mainly due to SGD. Right: a perpendicular profile in front of the dunes of Wenduine (Belgium), resistivity increases only slightly with decreasing water depth.



Figure 3: The CMD-MiniExplorer ECa mapping (left) versus rECa (right), both with CMD3 (23 February 2018). Copyright: Microsoft Corporation, DigitalGlobe, and CNES, 2019.

5

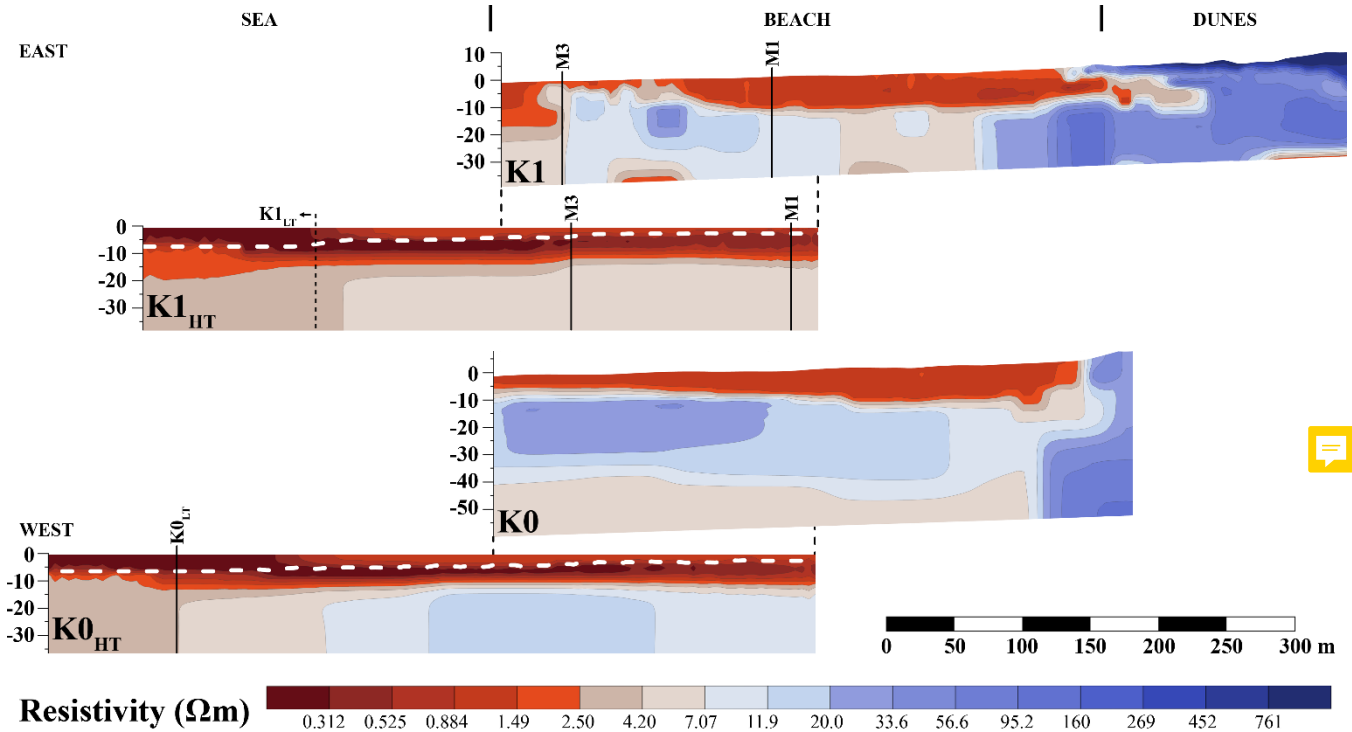


Figure 4: CRP and ERT profiles from in front of ‘De Westhoek’ nature reserve, perpendicular to the beach: K1 (7 March 2018, abs. error 2.80%), K1<sub>HT</sub> (30 May 2018, abs. error 1.57%), K0 (11 October 2018, abs. error 1.70%), K0<sub>HT</sub> (30 May 2018, abs. error 1.53%). The full lines represent intersections with other profiles (Figures 5 and 6), dotted line indicates where the low tide profile K1<sub>LT</sub> starts (Figure 5), profile numbering based on Lebbe (1981), “HT” stands for high tide, and the water depth is in mTAW (relative to the reference level of Belgium).

5

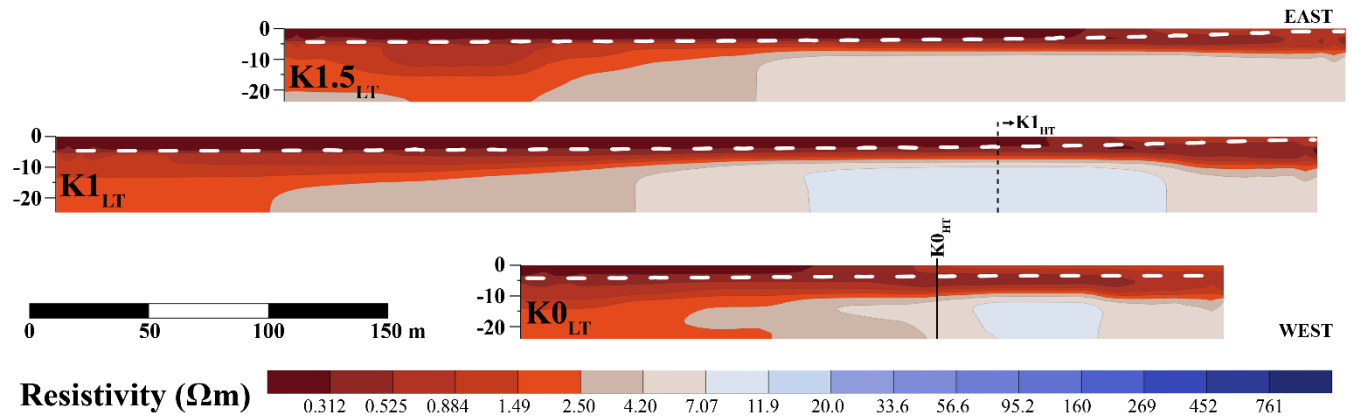


Figure 5: CRP profiles from the Westhoek, perpendicular to the beach (22 May 2019): K1.5<sub>LT</sub> (abs. error 0.78%), K1<sub>LT</sub> (abs. error 0.67%), and K0<sub>LT</sub> (abs. error 1.15%). Profile numbering based on Lebbe (1981), “LT” means low tide, and water depth in mTAW.

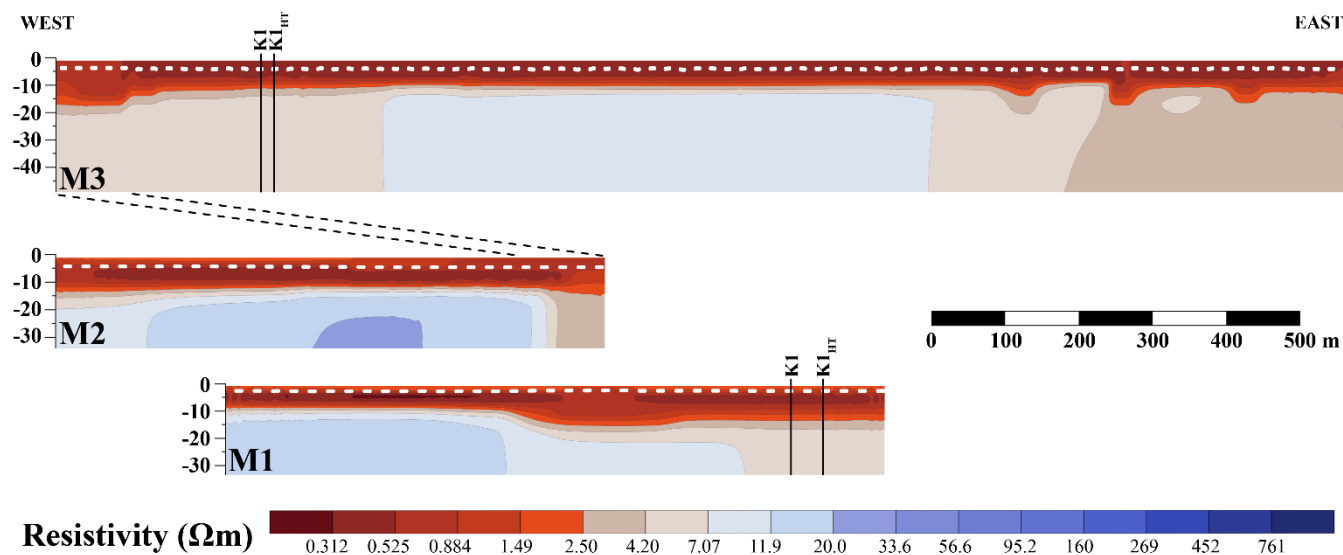
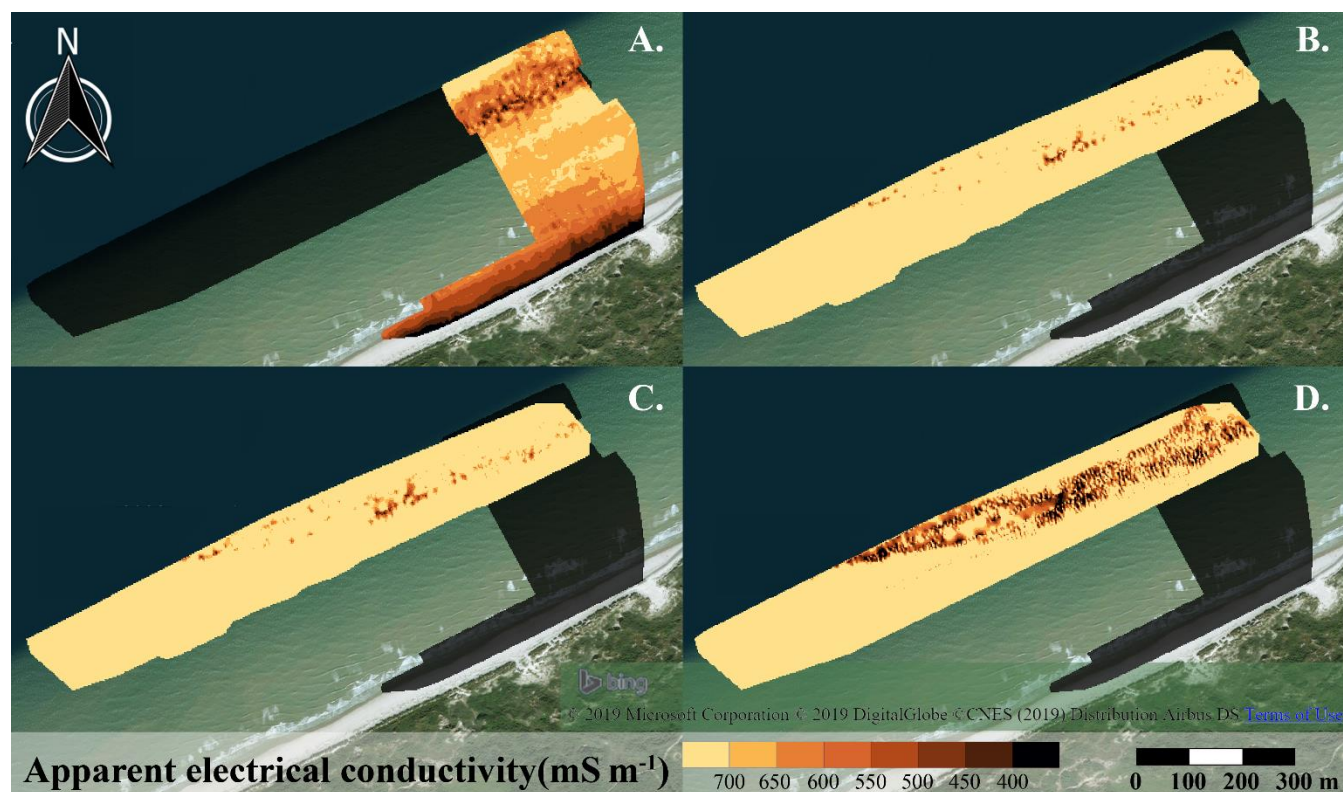


Figure 6: CRP profiles parallel to the beach, taken during high tide (30 May 2018): M3 (abs. error 1.39%), M2 (abs. error 1.77%), M1 (abs. error 0.83%). Full lines represent intersections with the perpendicular profiles (Figure 4) and water depth in mTAW.



5



**Figure 7: FDEM data: A. rECa (CMD-MiniExplorer) using CMD3 (23 February 2018); B., C., and D.: rECa (DUALEM-421S) using respectively HCP1, PRP4, and HCP4 configurations (27-28 September 2018). Note that another colour scale is used compared to the other figures. Copyright: Microsoft Corporation, DigitalGlobe, and CNES, 2019.**

5

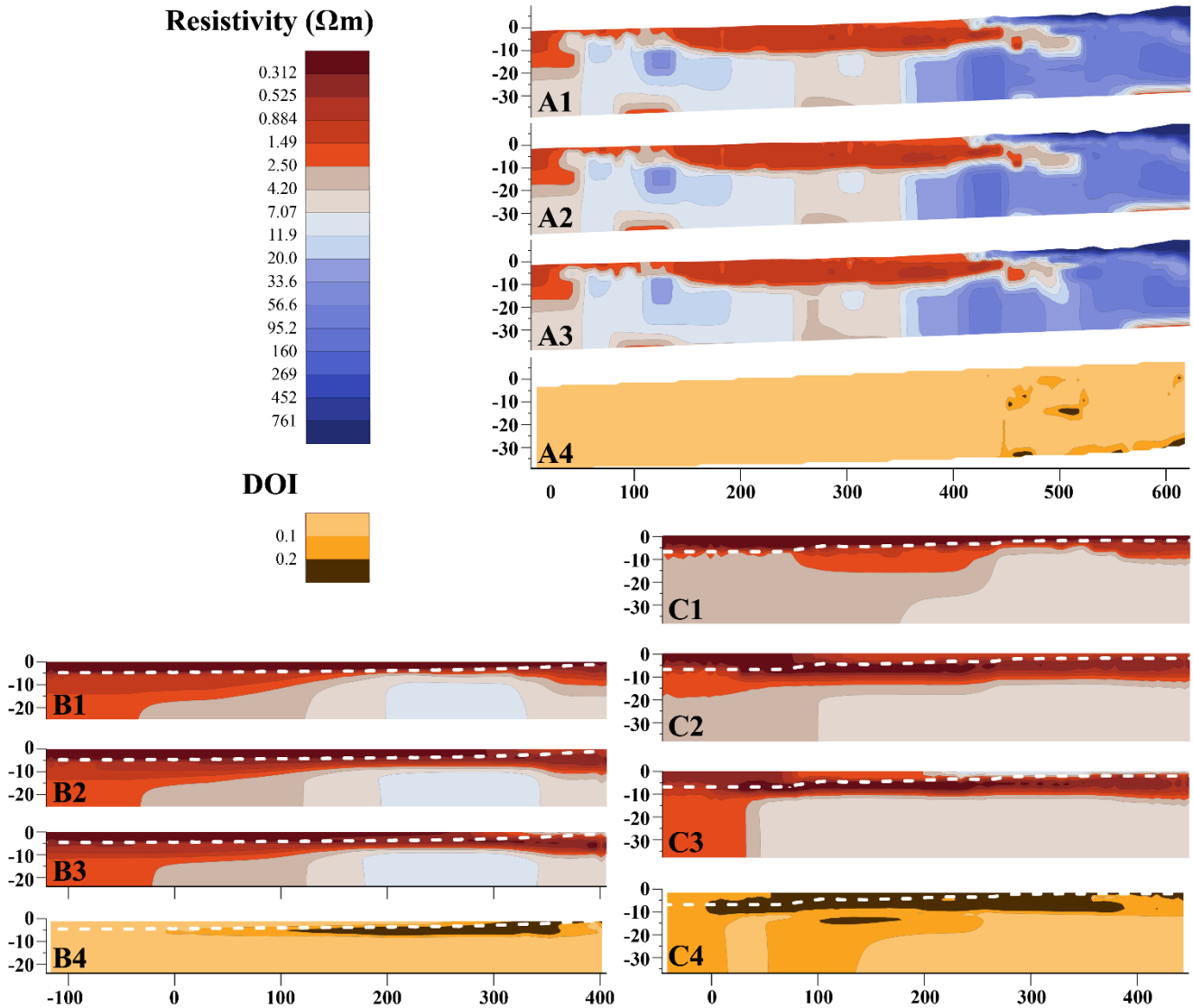


**Figure 8: Validation of the inversion models at 1 km from the Belgian-French border. A, K1 land ERT profile: models A1 (reference resistivity 0.4926), A2 (reference resistivity 4.926), and A3 (reference resistivity 49.26) have an abs. error of 2.8%, and the DOI (A4); B, K1<sub>LT</sub>, CRP low tide profile: B1 (reference resistivity 0.1096, abs. error 0.76%), B2 (reference resistivity 1.096, abs. error 0.67%), B3 (reference resistivity 10.96, abs. error 1.36%), and the DOI (B4); C, K1<sub>HT</sub>, CRP profile taken at high tide: C1 (reference resistivity 0.1263, abs. error 1.65%), C2 (reference resistivity 1.263, abs. error 1.57%), C3 (reference resistivity 12.63, abs. error 1.84%), and the DOI (C4).**

10